Composites: Part B 73 (2015) 82–88

Contents lists available at ScienceDirect

Composites: Part B

journal homepage: www.elsevier.com/locate/compositesb

Direct joining of carbon-fiber–reinforced plastic to an aluminum alloy using friction lap joining

Kimiaki Nagatsuka [a,*], Shoichiro Yoshida [a], Atsuki Tsuchiya [b], Kazuhiro Nakata [a]

[a] Joining and Welding Research Institute, Osaka University, 11-1, Mihogaoka, Ibaraki, Osaka 567-0047, Japan
[b] Toray Industries, Inc., 9-1, Oe-cho, Minato-ku, Nagoya 455-8502, Japan

ARTICLE INFO

Article history:
Received 10 October 2014
Received in revised form 8 December 2014
Accepted 15 December 2014
Available online 20 December 2014

Keywords:
Friction lap joining
A. Polymer-matrix composites (PMCs)
B. Mechanical properties
B. Microstructures
E. Joints/joining

ABSTRACT

A carbon-fiber–reinforced thermoplastic (polyamide 6 with 20 wt.% carbon fiber addition) and an aluminum alloy (A5052) were joined using friction lap joining. The joint characteristics were evaluated to investigate the effects of A5052 surface treatments and the joining speed on the joint properties. Carbon-fiber–reinforced thermoplastic and A5052 were joined via an interfacial magnesium oxide layer. Surface grinding of the A5052 generated the aluminum hydroxide on the alloy surface and increased the tensile shear strength of the joint. The tensile shear strength increased as the joining speed increased from 100 to 1600 mm min^{-1}, and decreased thereafter.

1. Introduction

Polymeric/plastic materials are extensively utilized in many industries to achieve significant weight reduction, superior thermal and electrical insulation, design flexibility, and good corrosion resistance in manufactured components [1]. Carbon-fiber–reinforced plastics (CFRPs) have been introduced recently as structural materials in aircraft and automobiles, where they can reduce fuel consumption and CO_2 emissions by virtue of their light weight and remarkable mechanical properties [2–6]. In particular, carbon-fiber–reinforced thermoplastics (CFRTPs), made by adding carbon fibers to thermoplastic matrix materials such as polyamide, polyphenylene sulfide, and polyethylene have large specific tensile strengths compared to conventional metal materials and retain several key polymer materials properties. In addition, CFRTPs are highly processable since they can be formed using mold-injection methods [4–6]. Because of these advantages, dissimilar joining techniques for attaching CFRTPs to metals have been developed to expand the range of applications for CFRTPs and improve their manufacturing production and performance characteristics. However, the direct joining of CFRTPs to metal materials is difficult because of their fundamentally different chemical and physical properties [1,7].

Adhesive bonding and mechanical fastening are conventional processes for joining plastic materials, including CFRTPs, to metals [8–14]. However, these joining techniques have several drawbacks. Adhesive bonding produces environmental pollutants in the form of volatile organic compounds emitted during processing, requires long processing times for efficient bonding, and provides non-uniform and/or insufficient joint strengths. Mechanical fasteners not only produce stress concentrations, reduce air-tightness, and increase weight, but are also not suitable for many mass production schemes. Other approaches to the direct joining of plastic materials to metals have been investigated recently, such as a laser joining [7,12–17], ultrasonic welding [18–20], and friction spot joining [21,22]. Katayama et al. [12–16] developed a laser-based direct-joining process for metals and plastics. In this process, a metal and a plastic material are joined using the heat produced by laser irradiation of the metal substrate. This technique can join plastics and various kinds of metal materials directly at high speed. The limitations of this process include the high cost of the laser unit, deterioration of the joined materials, and the complex welding parameters involved. Ultrasonic lap welding and friction spot joining can also form joints between plastics and metals; however, the dimensions and joint geometry are restricted.

These problems can be solved or mitigated by employing the friction lap joining (FLJ) method, which is a novel direct joining method capable of joining plastic materials, including CFRTPs, to

* Corresponding author. Tel.: +81 6 6879 8668; fax: +81 6 6879 8658.
E-mail addresses: nagatuka@jwri.osaka-u.ac.jp (K. Nagatsuka), shoichi@jwri.osaka-u.ac.jp (S. Yoshida), Atsuki_Tsuchiya@nts.toray.co.jp (A. Tsuchiya), nakata@jwri.osaka-u.ac.jp (K. Nakata).

http://dx.doi.org/10.1016/j.compositesb.2014.12.029
1359-8368/

metals [23,24]. Fig. 1 shows the FLJ technique schematically. FLJ can be carried out using a friction stir welding (FSW) apparatus [25,26], and uses the heat energy generated by friction between the rotating tool and metal surface. A reusable rotating tool is pressed into the surface of the metal plate and dragged along the overlap region. The tool not only heats the materials to be joined but also applies pressure at the joint interface [23,24]. The appearance of a FLJ joint is similar to that of a FSW joint. The tool in FSW incorporates a stirring probe to assist material flow, but the tool in FLJ does not. Heat transfer (via conduction) from the heated metal to the plastic component produces a narrow melted region in the plastic material near the interface. Joining of the metal and the plastic is complete after the melted plastic, under pressure produced by the contact with the metal substrate, solidifies. Given these advantages, FLJ has the potential to generate interfaces with strong joint strengths without any damage to the base materials, high-cost apparatus, or design limitations imposed on the joint geometry. In addition, there are significantly fewer joining parameters in FLJ – only four variables: tool dimension, rotation speed, plunge depth, and joining speed have to be controlled – and FLJ is an energy-saving and environmentally friendly process. This technique would further expand the applications for plastic materials, including CFRTPs, combined with metals.

As the metal in a joined plastic/metal component, Al alloys offers weight reduction, high strength, and good formability, all of which are important considerations in the fabrication of automobiles and aircraft [26]. The purpose of this study was to confirm the possibility of directly joining CFRTPs and Al alloys using the FLJ technique and to evaluate the joint characteristics, including the joint strength, interface structure, and fracture behavior. Also, the effect of grinding the surface of the Al alloy on the joint strength was investigated, since the condition of the surfaces plays an important role in the direct joining of these materials [17,27]. Finally, the effect of the joining speed during FLJ was investigated using ground Al specimens. The joining speed is an important parameter which affects both the interface temperature and heating interval, as well as the industrial applicability of the process.

2. Material and methods

Experiments were carried out on injection-molded CFRTP plates (80 mm × 80 mm × 3 mm) made of polyamide 6 with 20 wt.% short-cut carbon fiber addition and A5052 Al alloy plates (150 mm × 75 mm × 2 mm) with a composition of 2.4 mass% Mg and 0.18 mass% Cr. The diameter and length of these carbon fibers were 10 μm and approximately 500 μm, respectively. The A5052 plates were used in both the unground/as-received condition and after wet-grinding with #800 emery paper. The surfaces of both the unground and ground A5052 plates were analyzed using X-ray photoelectron spectroscopy (XPS, Quantera SXM, Physical Electronics, Inc., Chanhassen, MN, USA).

The CFRTP plates exhibit an anisotropic tensile strength due to the orientation of the carbon fibers. To determine these strengths, the CFRTP plates were cut into dumbbell-shaped tensile specimens parallel to both the flow direction (FD) and the transverse direction (TD) in injection molding. Tensile tests were carried out using a precision universal tester at a crosshead speed of 0.5 mm min^{-1}. The average tensile strengths of the CFRTP were 140 MPa in the FD and 117 MPa in the TD. The FD of the CFRTP plate was oriented toward the joining line. Two CFRTP plates were placed in a row and the ground surface of A5052 plate was placed facing the CFRTP plates, as shown in Fig. 1. FLJ was used to join the A5052 plate to the two CFRTP plates using a rotating tool made of SKD tool steel. The tool had 15 mm diameter shoulder (without probe) and was tilted at an angle 3° forward from the vertical. A tool plunge depth of 0.9 mm and a tool rotation speed of 2000 rpm were used, as determined by preliminary experiments. Different joining speeds in the range 100–2000 mm min^{-1} were employed for the ground-A5052/CFRTP joints, but the speed was fixed at 1600 mm min^{-1} for the unground-A5052/CFRTP joints. The temperature during FLJ was monitored using a K-type thermocouple inserted at the ground-A5052 plate/CFRTP plate interface at the center of the joined area. The normal load on the tool during travel was monitored by force sensors (9047C, Kistler Japan Co., Ltd., Tokyo, Japan).

The FLJ-joined specimens were cross-sectioned and mounted in epoxy resin before they were ground with #220 SiC paper and polished with diamond paste. Observations of the macrostructure and microstructure of the joined interface were then performed using optical microscopy (OM) and a transmission electron microscopy (TEM, 2100F, JEOL, Ltd., Tokyo, Japan).

A gel permeation chromatography (GPC) analysis was carried out to evaluate the molecular weight changes in the polyamide 6 in the CFRTP by sampling the CFRTP near the FLJ joint in samples joined at speeds of 100 and 1600 mm min^{-1}. The GPC analysis employed a differential refractometer detector (Shodex RI104, Showa Denko K. K., Tokyo, Japan); the column (Shodex HFIP-606 M, Showa Denko K. K., Tokyo, Japan) was held at a temperature of 313 K, and hexafluoroisopropyl alcohol with 5 mol m^{-3} of trifluoroacetic acid sodium salt at a flow rate of 3.3 mm^3 s^{-1} was used as the solvent. The molecular weight was determined relative to that of polymethyl methacrylate.

To evaluate the joint strength, the FLJ joints were cut into strips perpendicular to the joining direction with a width of 15 mm. Tensile shear tests were carried out using a precision universal tester at a crosshead speed of 0.5 mm·min^{-1}. Three strips were tested for each joining condition. The fracture surfaces of the tensile shear specimens were observed using OM, scanning electron microscopy (SEM), and energy dispersive X-ray spectroscopy (EDS).

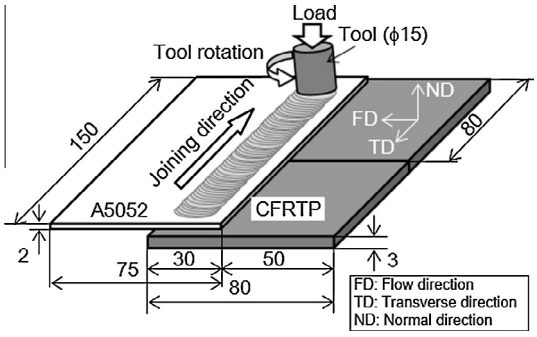

Fig. 1. Schematic illustration of the friction lap joining process indicating dimensions and directions. (All dimensions in mm.)

3. Results

3.1. Effect of grinding the A5052 plate

Fig. 2 shows the bright-field images and distributions of the elements Al, Mg, O, and C at the interface for both the unground- and ground-A5052/CFRTP joints. No voids or gaps were observed at the adhered interface. The CFRTP and A5052 alloy were joined via an oxide layer that consisted of Mg and O. A selected-area diffraction analysis identified the oxide layer as MgO.

Fig. 3 shows the tensile shear strengths of the unground- and ground-A5052/CFRTP joints and the macrostructures of the matching fracture surfaces of the unground A5052, ground A5052, and CFRTP surfaces. The tensile shear strength of the

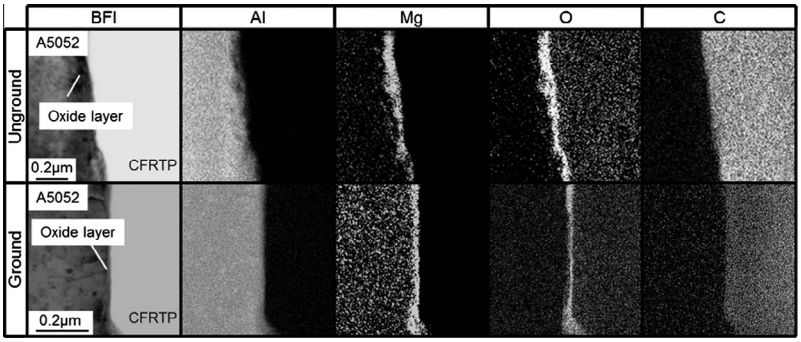

Fig. 2. TEM bright-field images and elemental distribution maps of Al, Mg, O, and C at the unground- and ground-A5052/CFRTP interfaces.

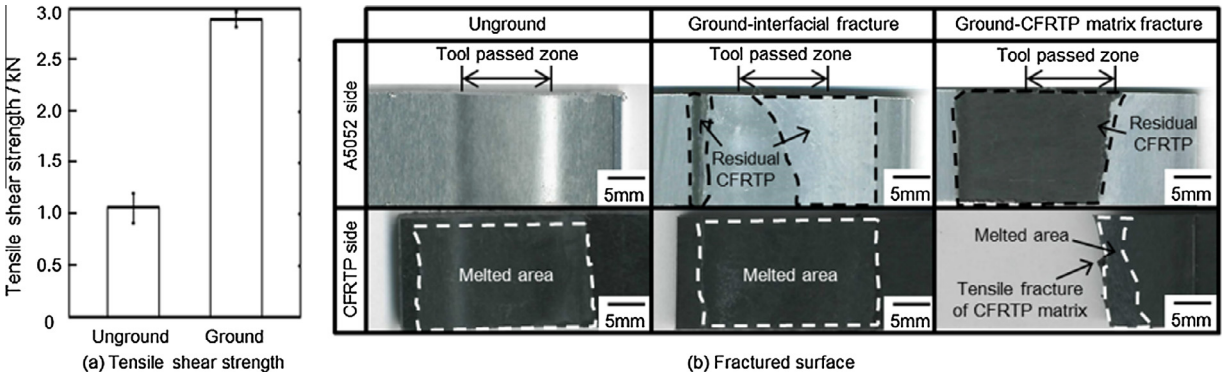

Fig. 3. (a) Tensile shear strength of the unground- and ground-A5052/CFRTP joints, and (b) the associated macrostructures of the opposing fracture surfaces.

unground-A5052/CFRTP joint was 1.0 kN; the strength was increased significantly by the grinding treatment to 2.9 kN. One specimen from a ground-A5052/CFRTP joint fractured entirely in the CFRTP plate. However, almost all of the joints fractured near the A5052/CFRTP interface. Regarding the joints with interfacial fractures: the rectangular areas enclosed by dashed lines on the macrographs of the CFRTP side indicate the melted area of polyamide 6, the matrix material of the CFRTP, which spread over the tool-passed zone. For the unground-A5052/CFRTP joints, the presence of CFRTP was not observed on the A5052, and a smooth, bright surface was observed together with the smooth surface of the CFRTP side. This is an indication that the unground-A5052/CFRTP joint fractured only at the interface of the two materials. On the other hand, for the ground-A5052/CFRTP joint, residual CFRTP adhered to the A5052 was present on the fractured surface of theA5052, though a smooth, bright zone without the residual CFRTP was also observed. The ground-A5052/CFRTP joint partially fractured through the CFRTP, including both the matrix and the carbon fibers, even though the joint fractured macroscopically at the interface. The unground-A5052/CFRTP joints possessed weak interfacial strengths, and therefore the fracture mainly occurred at the interface between the materials. Grinding the A5052 increased the joint strength, and fracture occurred at least partially in the CFRTP. Thus, grinding the surface of the A5052 plate prior to joining improves the joint strength.

Table 1 lists the results of the elemental composition determination (calculated from the XPS analysis) as well as the O_{Al}/Al ratios of the surfaces of the unground and ground A5052 plates prior to the FLJ experiments. O_{Al} is the estimated quantity of O that reacted with Al. Al, O, Mg, and C were detected on both surfaces. C was present as a contamination layer, and Al and Mg were the primary elements comprising the A5052 alloy. A wave analysis of the

Table 1
Results of the XPS analysis and the O_{Al}/Al values for unground and ground A5052.

	Element/at.%					O_{Al}/Al
	Al	O	Mg	C	O_{Al}[a]	
Unground	16.8	35.9	3.7	43.6	32.2	1.9
Ground	15.2	45.0	1.3	38.5	43.7	2.9

[a] O_{Al} = O–Mg.

Al2p and Mg2p signals indicated that Al existed mainly as Al_2O_3 and $Al(OH)_3$, and Mg existed as MgO. However, it is difficult to distinguish the Al_2O_3 component from the $Al(OH)_3$component with the Al 2p wave analysis alone because the difference in binding energy of Al2p between Al_2O_3 and $Al(OH)_3$ is very small; the binding energies of Al_2O_3 and $Al(OH)_3$ have been reported as 74.1–74.6 eV and 74.3–74.5 eV, respectively [28,29], and this difference was the same order of the magnitude as the experimental precision of the XPS instrument. The ratio of Al to O is generally used to distinguish the Al_2O_3 and $Al(OH)_3$ so the O_{Al}/Al value was calculated for this purpose [28]. O_{Al}, defined as the quantity of O that reacted with Al, was calculated by subtracting the Mg content from that of O, based on the assumption that all of the Mg reacted with O to form MgO. The theoretical O_{Al}/Al values for Al_2O_3 and $Al(OH)_3$ were calculated to be 1.5 and 3, respectively. As the results of the XPS analysis show, the value of O_{Al}/Al increased from 1.9 to 2.9 after surface grinding. These results indicated that the form of Al in the alloy changed from Al_2O_3 to $Al(OH)_3$ during wet grinding.

3.2. Effect of joining speed of FLJ for ground A5052/CFRTP

Fig. 4 shows the temperature history during FLJ of the ground-A5052/CFRTP joint produced at joining speeds of 100 and

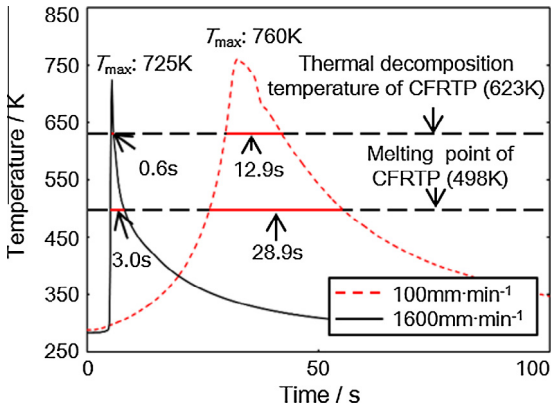

Fig. 4. Temperature histories during FLJ of ground-A5052/CFRTP joints fabricated at joining speeds of 100 and 1600 mm min^{-1}.

1600 mm min^{-1}. The temperature of the joint interface rapidly increased as the rotating tool approached the midway measurement point. Maximum temperatures of 760 K and 725 K were obtained at joining speeds of 100 mm min^{-1} and 1600 mm min^{-1}, respectively. These were above the melting temperature (approximately 498 K) and thermal decomposition temperature (approximately 623 K) of polyamide 6. The time interval during which melting and/or thermal decomposition could occur (i.e., the span of time over which the temperature of the CFRTP exceeded these critical temperatures) changed with the joining speed. The decrease in joining speed from 1600 mm min^{-1} to 100 mm min^{-1} increased the melting interval from 3.0 to 28.9 s and the thermal-decomposition interval from 0.6 to 12.9 s.

The average normal forces on the tool during travel were 0.6 kN at a joining speed of 100 mm min^{-1} and 4.3 kN at a speed of 1600 mm min^{-1}. The A5052 plate softened near the tool-passed zone, and the area of melted CFRTP expanded when the joining speed was reduced as a result of the temperature change shown in Fig. 4. Hence, the magnitude of the tool normal force decreased at constant tool plunge depth (0.9 mm). Fig. 5(a) and (b) show the cross-sectional macrostructure of the ground-A5052/CFRTP joints and the microstructure of the CFRTP region of the joints, respectively, for joints with joining speeds of 100, 800, 1600, and 2000 mm min^{-1}. Continuous ground-A5052/CFRTP joints were obtained at all of the joining speeds employed in this study. With decreasing joining speed, the concave-downward deformation of the A5052 plate, which pressed against the underlying CFRTP plate, increased in the tool passed zone. Thus, the thickness of CFRTP plate also decreased, and the estimated melted-zone size in the CFRTP enlarged, as indicated in Fig. 5(b) by dashed lines in each macrograph. Given these deformations in the A5052 plates, the thinning of the CFRTP should depend not on the tool normal force, but on the temperature, as the tool force decreased with decreasing joining speed.

Fig. 5(b) also shows the cross-sectional microstructure of as-injected CFRTP for comparison with those of the FLJ-processed joints. The as-injected CFRTP retains the structure as it was after injection molding, and this structure contains carbon fibers naturally oriented parallel to the flow direction of injection molding at both the top and bottom surface zones and perpendicular in the middle zone. After FLJ, however, the carbon fiber orientation was disturbed in the melted area as the carbon fibers moved according to the flow of the melted polyamide 6 outward from the tool-passed zone. Voids were observed beneath the interface in the melted zone of CFRTP regardless of the joining speed, and there was no relationship between the joining speed and the volume and quantity of the voids. Volatile products such as H_2O and CO_2 are generated by the thermal decomposition of polyamide 6 at temperatures over 573 K [7,30,31], and these voids formed as a result. The voids in the melted area would also be pushed outward from the tool-passed zone by the flow of melted polyamide 6, therefore, no relationship between the joining speed and void quantity would be observed in the tool-passed zone. Table 2 lists the weight-averaged molecular weight of polyamide 6 in the CFRTP near the interface of the A5052/CFRTP joint and in the as-injected CFRTP, as measured by GPC analysis. The weight-averaged molecular weight decreased from 34,700 to 27,000 during FLJ heating at a joining speed of 100 mm min^{-1}. On the other hand, at a joining speed of 1600 mm min^{-1}, it only decreased from 34,700 to 34,000, almost maintaining the same weight as as-injected CFRTP. For lower joining speeds such as 100 mm min^{-1}, the CFRTP was subjected to higher temperatures for longer intervals, and the thermal decomposition of polyamide 6 was thereby promoted.

Fig. 6 shows relationship between the joining speed and the resulting tensile shear strength of the joint. In Fig. 6(a), a black circle (●) indicates the fully tensile fracture of the CFRTP plate itself, a cross (×) indicates a purely interfacial fracture, and a white circle (○) means that the fracture mode was mixed. The cross (×) is used in cases where the area fraction of the residual CFRTP observed on the fractured surface of A5052 in the tool-passed zone was lower

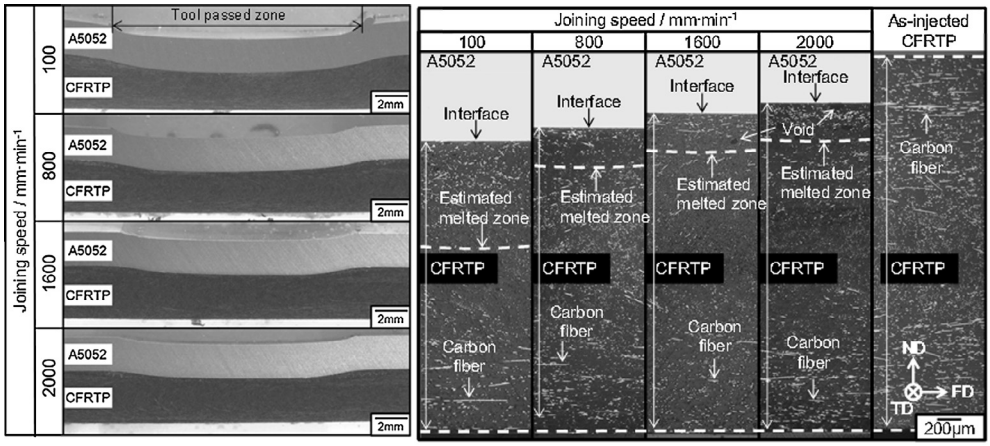

(a) Macrostructure of the joint (b) Microstructure of the CFRTP area

Fig. 5. (a) Cross-sectional macrographs of the ground A5052/CFRTP joints, and (b) cross-sectional micrographs of the CFRTP regions of the joints processed at joining speeds ranging from 100 to 2000 mm min^{-1}.

Table 2
Weight-averaged molecular weight of polyamide 6 in the CFRTP near the interface of the A5052/CFRTP joint and in the as-injected CFRTP, as measured by GPC analysis.

Joining speed	Weight-average molecular weight[a], Mw/10^4
100 mm min^{-1}	2.70
1600 mm min^{-1}	3.40
As-injected CFRTP (Polyamide 6)	3.47

[a] Relative to polymethyl methacrylate standards.

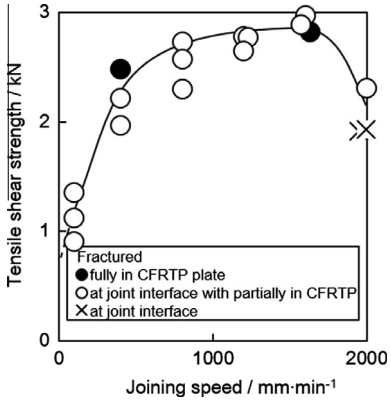

Fig. 6. The relationship between joining speed during FLJ and the tensile shear strength of the joints.

than 10%. The tensile shear strength increased with the joining speed up to 1600 mm min^{-1}, and then decreased. The maximum tensile shear strength of the joint fabricated at 1600 mm min^{-1} was 2.9 kN. Almost all of the FLJ joints fractured near the A5052/CFRTP interface. However, complete fracture in the CFRTP plate itself was observed in joints made with a joining speed of 400 and 1600 mm min^{-1}. The maximum tensile strength of the joints at that underwent the fully tensile fracture of the CFRTP plate itself were 58 and 60 MPa for joining speeds of 400 and 1600 mm min^{-1}, respectively. These strengths were lower than those in the FD (140 MPa) and TD (117 MPa) directions of the as-injected CFRTP. A thin residual CFRTP layer was observed in the tool-passed zone on the fractured surface of the A5052 at all of the joining speeds except 2000 mm min^{-1}. The melted area of the CFRTP corresponding to the joined area was observed on the fractured surface of the CFRTP, and this enlarged with decreasing joining speed. The voids were also observed primarily in this area. The joint tensile shear strength decreased, regardless of the size of the joined area, with decreasing joining speed.

Fig. 7 shows the secondary electron images and elemental distribution maps of Al, C, and O for the microstructure on the A5052 side of the fractured A5052/CFRTP joint made with a joining speed of 1600 mm min^{-1}. The SEM observations demonstrated that the morphologies of these fracture surfaces fell into three categories – regions 1, 2, 3 – corresponding to the images (a)–(c) in Fig. 7. Fig. 7(d)–(f) are high magnification images of the structures in (a)–(c), respectively. In region 1, bulk CFRTP was not observed; however, the presence of residual C was detected along the grinding scratches in the high magnification image in Fig. 7(d). This indicated that the surface roughness generated during the grinding contributed to the increase in joint strength via the anchor effect. In region 2, bulk CFRTP, featuring smooth surface features, was observed. These smooth features corresponded to the void surface, and therefore it is likely that the fracture would pass through this region. Bulk CFRTP was also observed in region 3. However, the fractured morphology was much different from that in region 2. A rough surface with exposed carbon fibers was observed in region 3, which corresponded to CFRTP plate fracture. The fracture passed through the CFRTP alone near the interface in region 3.

Fig. 8 shows the secondary electron images and classification of fracture surface morphologies of A5052 for joints formed at joining speeds of 1600 mm min^{-1}. Table 3 lists the area fractions of (1) joint interface fracture, (2) CFRTP void fracture, and (3) CFRTP-itself fracture in the tool-passed zone, determined from the secondary electron images of the fracture surface on A5052 of fractured joints formed at joining speeds of 100, 1600, and 2000 mm min^{-1}. In the joint formed at the joining speed of 1600 mm min^{-1}, fracture occurred in the void region of the CFRTP (region 2) and in the CFRTP itself (region 3) in addition to the joint interface (region 1). At lower joining speeds, the tensile shear strength of the joints was lower than that at a joining speed of 1600 mm min^{-1}, though the fraction of the void-affected area (region 2) decreased from 11.4% to 6.2% as the joining speed decreased from 1600 to 100 mm min^{-1}. Thus, void formation was not the primary cause of the decrease in the tensile shear strength at low joining speeds. On the other hand, the area fraction of the CFRTP-itself fracture (region 3) increased with decreasing joining speed from 1600 down to 100 mm min^{-1}. In contrast, fracture in joints made with a joining speed of 2000 mm min^{-1} almost always occurred at the joint interface (region 1).

4. Discussion

As indicated by the data in Fig. 3, surface grinding of the A5052 increased the strength of the A5052/CFRTP FLJ joints. The presence of the surface oxides Al_2O_3 and MgO and the hydroxide $Al(OH)_3$ affect the joining of the A5052 and the polyamide 6 in the CFRTP, which is the result of hydrogen bonding between NH and CH groups in polyamide 6 and –O or –OH groups in the oxide and hydroxide compounds [17,32–34], respectively, on the A5052 surface. The hydroxide groups strongly contribute to the wetting of the A5052 surface by the molten polyamide 6 [17,32]. Therefore, surface grinding resulted in an increase of the joint strength. However, Al_2O_3 and $Al(OH)_3$ layers on the surface of the A5052 were deoxidized during the FLJ process; thus, only MgO was detected at the interface of the unground- and ground-A5052/CFRTP joints, as shown in Fig. 2. In addition, the anchor effect [34] and the elimination of the contaminant layer [32] would also increase the strength of joints with a ground surface. The linear scratches produced during grinding increased the surface roughness; the arithmetic mean roughness changed from 0.15 μm to 0.25 μm after the #800 wet grinding. The A5052 alloy and the CFRTP were mechanically joined across this rough surface via the anchor effect, and the joint strength was thereby enhanced. The surface contamination layer, which prevents the wetting of the A5052 surface by the melted CFRTP, was removed by grinding. During the joining of these two materials, good wetting would be obtained in a cleaned and would contribute to the formation of a strong joint.

Regarding the effect of joining speed (cf. Fig. 6), the tensile shear strength decreased with increasing joining speed from 1600 to 2000 mm min^{-1} and the fracture mainly occurred at the interface of A5052/CFRTP at a joining speed of 2000 mm·min^{-1}. This is caused by a lack of heat input; the temperature was too low and the melting interval was too short in the polyamide 6 so not enough wetting of molten CFRTP on the A5052 occurred. In contrast, the tensile shear strength increased with joining speed up to 1600 mm min^{-1}. The tensile shear strength of the joint decreased regardless of the increase in the area fraction of CFRTP-itself fracture. This is an indication that the deterioration of the CFRTP caused by thermal decomposition plays a critical role in the drop in joint strength at lower joining speeds. For lower

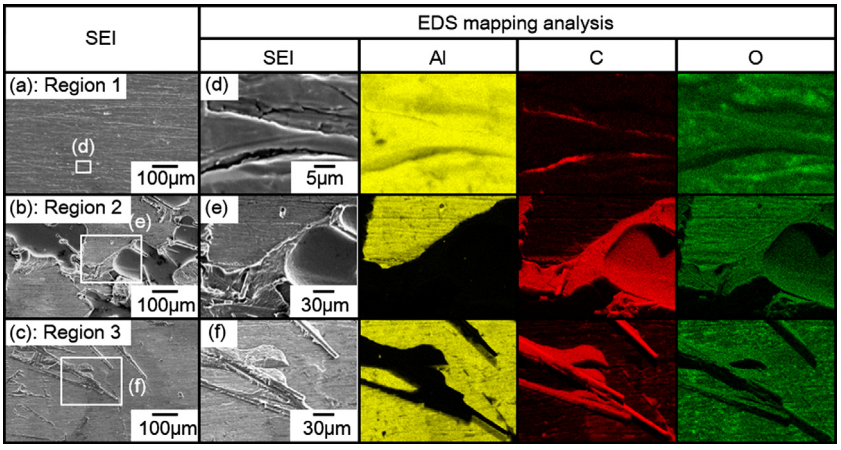

Fig. 7. Secondary electron images and elemental distribution maps of Al, C, and O in microstructure on A5052 side of fractured A5052/CFRTP joints produced at a joining speed of 1600 mm min^{-1}.

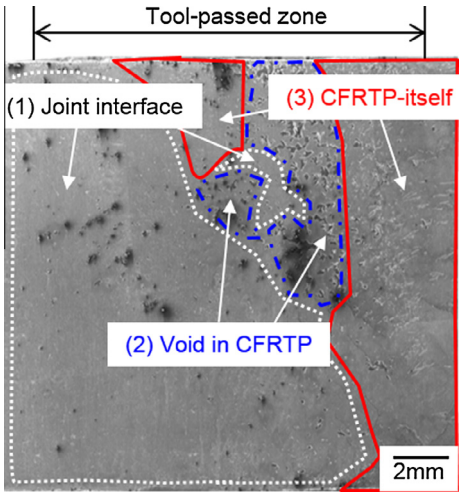

Fig. 8. Secondary electron images and classification of fracture surface characteristics on A5052 side of fractured joints formed at joining speeds of 1600 mm min^{-1}.

Table 3
Area fractions of (1) joint interface fracture, (2) CFRTP void fracture, and (3) CFRTP-itself fracture in the tool-passed zone, determined from the secondary electron images of the fracture surface on A5052 of fractured joints formed at joining speeds of 100, 1600, and 2000 min min^{-1}.

Fracture position	Joining speed (mm min^{-1})		
	100	1600	2000
(1) Joint interface	38.7	61.8	99.7
(2) Void in CFRTP	6.2	11.4	0.2
(3) CFRTP itself	55.1	26.8	0.1

joining speeds, such as 100 mm min^{-1}, the weight-averaged molecular weight of polyamide 6 was diminished by thermal decomposition because the CFRTP was subjected to higher temperatures for longer intervals, as shown in Table 2. This is the reason that the A5052/CFRTP joint strength decreased at the lower joining speeds. Additionally, from Fig. 6, the maximum tensile strength of the CFRTP-tensile-fractured joints was lower than those of the as-injected CFRTP. The reason why the tensile strength of CFRTP of the FLJ joint decreased to such a degree was that the heat input during FLJ caused (1) the generation of voids in CFRTP, (2) the reorganization of the carbon fiber orientations, and (3) the deterioration of the polyamide 6 CFRTP matrix.

5. Conclusions

The direct joining of a carbon-fiber–reinforced thermoplastic (CFRTP, polyamide 6 + 20 wt.% carbon fiber) and an Al alloy (A5052) was performed using friction lap joining (FLJ). The effects of surface roughening/grinding of theA5052 and the joining speed on the joint characteristics were investigated. We arrived at the following conclusions:

(1) The CFRTP and A5052 were joined via an MgO oxide layer.
(2) Grinding the A5052 surface generated the hydroxide $Al(OH)_3$, and the tensile shear strength of the FLJ joint increased from 1.0 to 2.9 kN with this surface treatment.
(3) The maximum temperature of the interface during FLJ increased from 725 to 760 K, and the time available for melting and/or thermal decomposition of the CFRTP increased (from 3.0 to 28.9 s and from 0.6 to 12.9 s, respectively), as the joining speed decreased from 1600 to 100 mm min^{-1}.
(4) The weight-average molecular weight of the polyamide 6 decreased during FLJ; however, it remained at the same level as the as-injected CFRTP at a joining speed of 1600 mm min^{-1}.
(5) The tensile shear strength increased with joining speed up to 1600 mm min^{-1}, then decreased at 2000 mm min^{-1}. The fracture surface of A5052 in the tool-passed zone was described by three basic characters: (i) joint-interface fracture, (ii) void fracture, and (iii) CFRTP-itself fracture. The area fraction of CFRTP-itself fracture increased from 0.1% to 55.1% as the joining speed decreased from 2000 to 100 mm min^{-1}.

Acknowledgements

This work was partly supported by the Innovative Structural Materials Project (Future Pioneering Project) of the Ministry of Economy, Trade and Industry of Japan.

References

[1] Stokes VK. Joining methods for plastics and plastic composites: an overview. Polym Eng Sci 1989;29:1310–24.
[2] Williams JC, Starke Jr EA. Progress in structural materials for aerospace systems. Acta Mater 2003;51:5775–99.
[3] Adam H. Carbon fibre in automotive applications. Mater Des 1997;18:349–55.
[4] Soutis C. Carbon fiber reinforced plastics in aircraft construction. Mater Sci Eng A 2005;412:171–6.

[5] Fu SY, Lauke B, Mäder E, Yue CY, Hu X. Tensile properties of short-glass-fiber- and short-carbon-fiber reinforced polypropylene composites. Compos Part A-Appl S 2000;31:1117–25.
[6] Razaei F, Yunus R, Ibrahim NA. Effect of fiber length on thermomechanical properties of short carbon fiber reinforced polypropylene composites. Mater Des 2009;30:260–3.
[7] Tan X, Zhang J, Shan J, Yang S, Ren J. Characteristics and formation mechanism of porosities in CFRP during laser joining of CFRP and steel. Compos Part B-Eng 2015;70:35–43.
[8] Arenas JM, Alía C, Narbón JJ, Ocaña R, González C. Considerations for the industrial application of structural adhesive joints in the aluminium–composite material bonding. Compos Part B-Eng 2013;44:417–23.
[9] Kabche JP, Caccese V, Berube KA, Bragg R. Experimental characterization of hybrid composite-to-metal bolted joints under flexural loading. Compos Part B-Eng 2007;38:66–78.
[10] Fink A, Camanho PP, Andrés JM, Pfeiffer E, Obst A. Hybrid CFRP/titanium bolted joints: performance assessment and application to a spacecraft payload adaptor. Compos Sci Technol 2010;70:305–17.
[11] Kumar SB, Sridhar I, Sivashanker S, Osiyemi SO, Bag A. Tensile failure of adhesively bonded CFRP composite scarf joints. Mater Sci Eng B 2006;132:113–20.
[12] Jung KW, Kawahito Y, Takahashi M, Katayama S. Laser direct joining of carbon fiber reinforced plastic to aluminum alloy. J Laser Appl 2013;25:032003.
[13] Wahba M, Kawahito Y, Katayama S. Laser direct joining of AZ91D thixomolded Mg alloy and amorphous polyethylene terephthalate. J Mater Process Technol 2011;211:1166–74.
[14] Katayama S, Kawahito Y. Laser direct joining of metal and plastic. Scr Mater 2008;59:1247–50.
[15] Kawahito Y, Katayama S. Innovation of laser direct joining between metal and plastic. Trans JWRI 2010;39:50–2.
[16] Jung KW, Kawahito Y, Katayama S. Laser direct joining of CFRP to metal or engineering plastic. Trans JWRI 2013;42:5–8.
[17] Hino M, Mitooka Y, Murakami K, Urakami K, Nagase H, Kanadani T. Effect of aluminum surface state on laser joining between 1050 aluminum sheet and polypropylene resin sheet using insert materials. Mater Trans 2011;52:1041–7.
[18] Balle F, Wagner G, Eifler D. Ultrasonic spot welding of aluminum sheet/carbon fiber reinforced polymer – joints. Mater Werks 2007;38:934–8.
[19] Balle F, Wagner G, Eifler D. Ultrasonic metal welding of aluminium sheets to carbon fibre reinforced thermoplastic composites. Adv Eng Mater 2009;11:35–9.
[20] Balle F, Eifler D. Statistical test planning for ultrasonic welding of dissimilar materials using the example of aluminum–carbon fiber reinforced polymers (CFRP) joints. Mater Werks 2012;43:286–92.
[21] Amancio-Filho ST, Bueno C, dos Santos JF, Huber N, Hage Jr E. On the feasibility of friction spot joining in magnesium/fiber-reinforced polymer composite hybrid structures. Mater Sci Eng A 2011;528:3841–8.
[22] Yusof F, Miyashita Y, Seo N, Mutoh Y, Moshwan R. Utilising friction spot joining for dissimilar joint between aluminium alloy (A5052) and polyethylene terephthalate. Sci Tech Weld Join 2012;17:544–9.
[23] Nakata K. International Patent Application No. PCT/JP2012/053839.
[24] Liu FC, Liao J, Nakata K. Joining of metal to plastic using friction lap welding. Mater Des 2014;54:236–44.
[25] Thomas WM, Nicholas ED. Friction stir welding for the transportation industries. Mater Des 1997;18:269–73.
[26] Chen YC, Nakata K. Friction stir lap joining aluminum and magnesium alloys. Scr Mater 2008;25:433–6.
[27] Molitor P, Barron V, Young T. Surface treatment of titanium for adhesive bonding to polymer composites: a review. Int J Adhes Adhes 2001;21:129–36.
[28] Kloprogge JT, Duong LV, Wood BJ, Frost RL. XPS study of the major minerals in bauxite: Gibbsite, bayerite and (pseudo) boehmite. J Colloid Interf Sci 2006;296:572–6.
[29] Tsuchida T, Takahashi H. X-ray photoelectron spectroscopic study of hydrated aluminas and aluminas. J Mater Res 1994;9:2919–24.
[30] Straus S, Wall LA. Pyrolysis of polyamides. J Res Nat Bur Stand 1958;60:39–45.
[31] Straus S, Wall LA. Influence of impurities of the pyrolysis of polyamides. J Res Nat Bur Stand 1959;63:269–73.
[32] The adhesion society of Japan. Secchaku-handbook, fourth ed. Tokyo: NIKKAN KOGYO SHIMBUN Ltd.; 2007: 834–63.
[33] Vellinga WP, Eising G, de Wit FM, Mol JMC, Terryn H, de Wit JHW, et al. Adhesion at Al–hydroxide–polymer interfaces: Influence of chemistry and evidence for microscopic self-pinning. Mater Sci Eng A 2010;527:5637–47.
[34] Wagner WC, Asgar K. Effect of interfacial variables on metal-porcelain bonding. J Biomed Mater Res 1993;27:531–7.